Void Growth in Glassy Polymers

Steenbrink, A.C.; van der Giessen, Erik

Published in:
International Journal of Damage Mechanics

DOI:
10.1177/105678959700600306

Publication date:
1997

Void Growth in Glassy Polymers: Effect of Yield Properties on Hydrostatic Expansion

A. C. STEENBRINK AND E. VAN DER GIESSEN*
Delft University of Technology
Laboratory for Engineering Mechanics
Delft, The Netherlands

ABSTRACT: Void growth in plastically deforming glassy polymers is investigated by means of a simple spherical symmetric model. This type of void growth occurs in cavitated polymer-rubber blends and, at a smaller scale, during craze initiation. The study serves to provide approximate values for the stresses required for elastic-viscoplastic void growth under hydrostatic loading conditions. The constitutive model accounts for features such as rate and temperature dependent yield, intrinsic strain softening after yield, and subsequent hardening due to molecular alignment at large deformations. The separate effects of these features on void expansion and the stress distribution are studied. Due to the relatively large strain at yield for most glassy polymers, elastic effects play an important role even at macroscopic yield. Therefore, predictions of the maximum stress are significantly lower than those based on rigid-plastic behaviour, especially for low void volume fractions.

1. INTRODUCTION

SIGNIFICANT PLASTIC DEFORMATION in glassy polymers or in glassy polymer-rubber blends usually leads to the formation and growth of voids. In the case of polymer-rubber blends, voids are formed as a result of cavitation within the rubber particles (see, e.g., References [1,2]). If the rubber modulus is low, the voided rubber particle can be idealized as a void, leaving a microporous material. The size of the voids is on the order of the initial particle diameter, i.e., ranging from 50 nm to 5 μm. Void formation can also occur at an even smaller size scale, as the beginning of a craze. The micromechanisms involved in craze nucleation and growth have been extensively discussed, e.g., in References [3–7]. From these studies, it appears that the first stage is void nucleation in a re-

*Author to whom correspondence should be addressed.

1056-7895/97/03 317-14 $10.00/0

gion of high dilatation or hydrostatic stress, which most likely occurs near defects or stress concentrations. Subsequently, void growth takes place. The fibrillar microstructure of the craze is presumed to be the result of multiplication of voids, for example, through a meniscus instability mechanism [5]. It is difficult to establish which of these three steps is the critical one for crazing. In both examples of voids in polymers, the dependence of void nucleation and growth on the stress state is a complicated one, but the hydrostatic component of stress is commonly considered to be the key quantity.

The micromechanical models that have been proposed in the references cited above usually employ quite simplistic models for the material behaviour. They have provided elementary qualitative understanding but have limited quantitative predictive power. Also, the role of plastic void growth around cavitated rubber particles in polymer-rubber blends is not well understood. To improve this, it is crucial to account for finite deformation effects as well as for advanced features of the material behaviour of amorphous polymers, like rate-dependent yield, intrinsic softening, and progressive strain hardening due to molecular orientation.

Recent numerical studies of void growth in glassy polymers [8,9] have demonstrated the importance of the typical softening and hardening behaviour, leading to plastic flow occurring by the initiation and propagation of shear bands. The resulting phenomenology of void growth has been found to be quite different from void growth in metals, which is by now well documented (see Reference [10] for a review). Nevertheless, a first, reasonable approximation of the macroscopic behaviour of the porous material could be obtained (see also Reference [11]) by a modification of Gurson's [12] model that was developed for metal plasticity. It has been shown in Reference [9] that an important modification is to account for elasticity, in view of the fact the yield strain in polymers is an order of magnitude larger than for metals. The assumption of rigid-plastic material behaviour for glassy polymers would lead to a severe overestimation of the macroscopic yield stresses compared to analyses based on the actual stress field. An approximate analytical solution for the problem of spherically symmetric void growth under hydrostatic tension for elastic-viscoplastic polymers without softening and hardening was then used in Reference [12] to modify Gurson's relation.

The present paper is an extension of this analysis to investigate the effects of intrinsic softening and progressive hardening of glassy polymers. Also, the behaviour in the limiting case of vanishingly small initial voids, leading to a cavitation instability, is discussed here.

2. PROBLEM FORMULATION

The analysis of spherical symmetric expansion of voids is greatly simplified if incompressible material behaviour is assumed. In that case, the strain field is kinematically determined and direct integration of the equilibrium equation

yields the remote hydrostatic stress. Material compressibility tends to reduce the overall stiffness [9], but qualitatively, the results are not influenced. Therefore, here too the assumption of incompressibility is maintained.

The approach followed here was briefly outlined in Reference [9] and will be elaborated on here. We consider a hollow sphere with initial dimensions a_0, b_0 for the inner and outer radius, respectively. The deformed geometry is specified by the corresponding quantities a and b, so that the current void volume fraction is $f = (a/b)^3$. Loading is applied by prescribing a fixed expansion rate $\dot{b}/b$ at the outer radius. Owing to spherical symmetry, the problem is a one-dimensional one, which is described here in terms of the radial coordinate r measured in the deformed configuration.

Throughout the deformation process, the principal directions of stretch coincide with the tangential and radial directions. Assuming incompressibility, the principal stretches are given by

$$\lambda_t = \frac{r}{r_0} \qquad \lambda_r = 1/\lambda_t^2 \tag{1}$$

when r_0 is the initial position of the material point currently at r. The corresponding tangential and radial logarithmic strain rates, $\dot{\epsilon}_t$ and $\dot{\epsilon}_r$, obey the incompressibility condition $\dot{\epsilon}_r + 2\dot{\epsilon}_t = 0$. The equivalent shear rate $\dot{\gamma}$ is now given as[1]

$$\dot{\gamma} = \sqrt{\dot{\epsilon}_r^2 + 2\dot{\epsilon}_t^2} = \sqrt{6}\dot{\epsilon}_t = \sqrt{6}\frac{\dot{r}}{r} \tag{2}$$

By virtue of incompressibility again, the stress state is completely determined by the equivalent shear stress $\tau = (\sigma_t - \sigma_r)/\sqrt{3}$, where σ_r and σ_t denote the radial and tangential components of the Cauchy stress tensor. These stress components are subject to the radial equilibrium condition

$$\frac{d\sigma_r}{dr} + \frac{2}{r}(\sigma_r - \sigma_t) = 0 \tag{3}$$

with boundary conditions $\sigma_r(a) = 0$ and $\sigma_r(b) = \sigma_m$. By integration of Equation (3), the applied hydrostatic stress σ_m can be expressed in terms of the current shear stress distribution inside the sphere as

$$\frac{\sigma_m}{s_0} = 2\sqrt{3}\int_a^b \left(\frac{\tau}{s_0}\right)\frac{dr}{r} \tag{4}$$

[1]The definition of $\dot{\gamma}$ used here differs from more usual definitions by a factor of $\sqrt{2}$ in order to be compatible with the definitions used in the constitutive model [14,15] (Section 2.1).

It is noted that the integral is taken over the current deformed configuration in order to account for the changes of the geometry during the deformation process.

The shear stress distribution, $\tau(r)$, to be substituted in Equation (4) follows from the response to the local shear process described by Equation (2) in accordance with the constitutive behaviour. The evaluation of Equation (4) at each stage of the deformation process is performed numerically.

2.1 Material Behaviour

The three-dimensional constitutive model used here and in References [8,9] is based on the original Haward-Thackray [13] model for plastically deforming polymers. A simple one-dimensional representation is shown in Figure 1. The initial elastic response is characterised by a linear spring. The plastic response is iconized by a dashpot, which represents rate and temperature dependent yield, and a parallel Langevin spring, which is used to account for the hardening effect caused by molecular alignment. For application to Equation (4), it is convenient to formulate the constitutive equations in terms of shear stresses. The shear stress τ is decomposed into a viscoplastic part τ_{vp} in the dashpot and a shear back stress τ_h to describe orientational hardening:

$$\tau = \tau_{vp} + \tau_h \tag{5}$$

For elastically incompressible material, the stress rate is related to the elastic part of the shear rate through

$$\frac{\dot{\tau}}{s_0} = c(\dot{\gamma} - \dot{\gamma}^p) \text{ with } c = \frac{\sqrt{2}}{3}\frac{E}{s_0} \tag{6}$$

where E is Young's modulus. For the plastic shear rate $\dot{\gamma}^p$, we adopt the yield model proposed by Argon [14], i.e.,

$$\dot{\gamma}^p = \dot{\gamma}_0 \exp\left[-\frac{As_0}{T}\left(1 - \left(\frac{\tau_{vp}}{s_0}\right)^{5/6}\right)\right] \tag{7}$$

where $\dot{\gamma}_0$ and A are material parameters, T is the absolute temperature, and s_0 is the shear strength. The effect of strain softening is incorporated in a phenomenological way by using a plastic shear dependent shear strength s instead of s_0 [15], governed by

$$\dot{s} = h(1 - s/s_{ss})\dot{\gamma}^p \tag{8}$$

The saturation value of s is s_{ss}, while h specifies the slope of the softening part. We assume that the deformation takes place isothermally. Furthermore, visco-

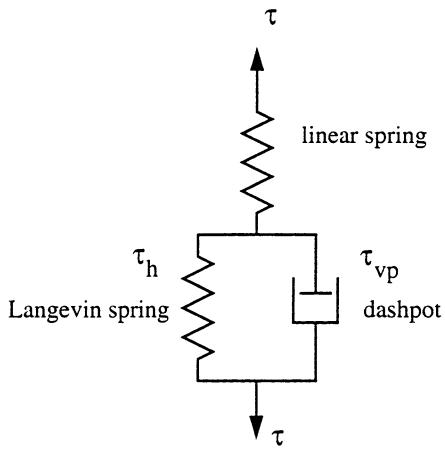

Figure 1. *Schematic, one-dimensional representation of the elastic-visoplastic material model.*

elastic effects are neglected; therefore, the elastic modulus E is interpreted as the ratio of yield stress and yield strain in uniaxial tension.

2.2 Orientation Hardening

The strain hardening effect for glassy polymers at large deformations is considered to be analogous to the stretching of the macromolecular network of a cross-linked rubber [13]. Several three-dimensional hardening models have been proposed [15–18], leading to constitutive equations for the back stress tensor **b**, specified in components b_i in the principal directions of the plastic stretches. For the calculation of the back stresses, we ignore the difference between total and plastic stretches (cf. [8,9]); the resulting deviation in the back stress levels remains small as long as the elastic strains remain small compared to the plastic strains. The equivalent shear stress τ_h in Equation (5) is given by the tangential and radial components of **b** as $\tau_h = (b_t - b_r)/\sqrt{3}$.

We employ two types of hardening models. The first type is based on the Neo-Hookean model for rubber elasticity, which is characterized by the following expression for the strain energy density W:

$$W = \frac{C^R}{2}(\lambda_1^2 + \lambda_2^2 + \lambda_3^2 - 3) \tag{9}$$

where C^R is the initial shear modulus and λ_i are the principal stretches. The principal components of the back stress tensor are determined, analogous to rubber elasticity theory, by

$$b_i^{(nh)} = \lambda_i \frac{\partial W}{\partial \lambda_i} \tag{10}$$

up to an unspecified superimposed hydrostatic pressure; the latter is irrelevant for the shear back stress τ_h and is therefore omitted. In this model, there is no limit to the extensibility of the material.

As opposed to this, the second type of hardening models is based on non-Gaussian rubber models which involve a limited extensibility. The full network model can be accurately represented by the following linear combination of the three- and eight-chain models [17]

$$\tau_h^{(full)} = (1 - \varrho)\tau_h^{(3)} + \varrho\tau_h^{(8)} \tag{11}$$

where ϱ controls the relative contributions of the respective hardening models, denoted by $\tau_h^{(3)}$ and $\tau_h^{(8)}$, and is being determined from the maximum principal stretch (λ_t in this case), through $\varrho = 0.85\,\lambda_t/\sqrt{N}$. Here, N is a hardening parameter that defines the finite extensibility of the network, with $\lambda_{max} = \sqrt{N}$. For $N \to \infty$, the network model reduces to the Neo-Hookean model.

Explicit expressions of the back stresses according to the various hardening models are given in Table 1, both in terms of components and equivalent shear back stresses.

3. RESULTS AND DISCUSSION

In order to study the effects of the various features of the stress-strain response of glassy polymers, we have considered five different parameter sets. The true stress vs. logarithmic strain in uniaxial tension at a constant strain rate $\dot{\epsilon} = 0.01s^{-1}$ for these five materials is shown in Figure 2.

The basic material parameter set is given by $E = 910$ MPa, $s_0 = 97$ MPa, $h = 500$ MPa, $\dot{\gamma}_0 = 2 \cdot 10^{15}\ s^{-1}$, $A = 240$ K/MPa, $T = 296$ K. For each material, the dataset is completed with the parameters given in Table 2. Material a is perfectly plastic, i.e., it neither exhibits softening nor hardening. The yield behaviour is still rate and temperature dependent as described by Equation (7). Material b shows softening, but no hardening. For material c, the hardening response is modelled with the full network model, taking $C^R = 5.7$ MPa and $N = 6.3$. In fact, this parameter set is the same as was used in previous studies [9] to represent the behaviour of polycarbonate. For material d, the hardening parameter is increased to $N = 12.6$, so as to represent a material with a lower entanglement density than material c. For material e, the hardening behaviour was taken to be Neo-Hookean, or equivalently taking $N \to \infty$. Consequently, the extensibility of material e is unlimited, whereas materials c and d have a limit stretch of $\lambda_{max} = \sqrt{N}$.

Table 1. Summary of constitutive equations for the back stress components (up to an arbitrary superimposed hydrostatic stress) and the equivalent shear back stress.

Model	b_i $\quad i$	$\tau_h = (b_t - b_r)/\sqrt{3}$
Neo-Hookean	$b_i^{(nh)} = \lambda_i \dfrac{\partial W}{\partial \lambda_i} = C^R \lambda_i^2$	$\tau_h^{(nh)} = C^R(\lambda_t^2 - \lambda_r^2)/\sqrt{3}$
Three-chain model [15]	$b_i^{(3)} = \dfrac{1}{3} C^R \sqrt{N} \lambda_i \beta_i$	$\tau_h^{(3)} = \dfrac{1}{3} C^R \sqrt{N}(\lambda_t \beta_t - \lambda_r \beta_r)/\sqrt{3}$
Eight-chain model [16]	$b_i^{(8)} = \dfrac{1}{3} C^R \sqrt{N} \dfrac{\lambda_i^2}{\lambda} \beta$	$\tau_h^{(8)} = \dfrac{1}{3} C^R \sqrt{N} \dfrac{\lambda_t^2 - \lambda_r^2}{\lambda} \beta/\sqrt{3}$

For the three-chain model, $\beta_i = \mathcal{L}^{-1}(\lambda_i/\sqrt{N})$, where $\mathcal{L}$ denotes the Langevin function defined as $\mathcal{L}(x) = \coth x - 1/x$.
For the eight-chain model $\beta = \mathcal{L}^{-1}(\lambda/\sqrt{N})$, with $\lambda = \sqrt{(1/3)(\lambda_1^2 + \lambda_2^2 + \lambda_3^2)}$.

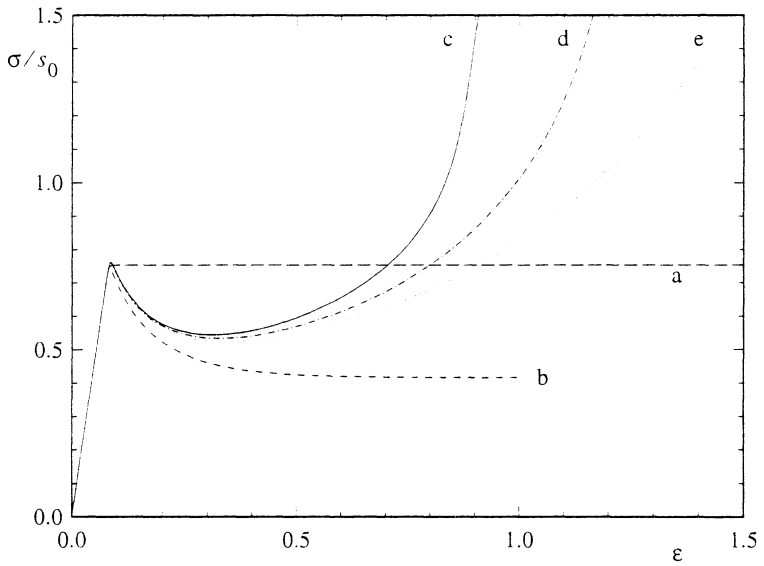

Figure 2. *Uniaxial stress response for the unvoided material using material parameter sets a to e.*

The macroscopic response of the hollow sphere will be represented here in terms of the hydrostatic stress σ_m at the outer boundary versus the logarithmic tangential strain at the inner boundary (as a convenient measure of deformation). The response to a remote strain rate of $\dot{b}/b = 0.01s^{-1}$ is shown in Figure 3 for three values of the initial void volume fractions ($f_0 = 10^{-6}$, 10^{-2} and 10^{-1}). As observed in Reference [9], the macroscopic stress σ_m eventually reaches a maximum, beyond which macroscopic softening occurs with continued void growth. The maximum is identified as the macroscopic yield stress Σ_m. The void expansion at which this macroscopic yield stress takes place is very sensitive to the initial void volume fraction f_0. However, in all cases, the overall dilatation at macroscopic yield remains small, i.e., $\ln(b/b_0) \ll 1$. Comparison of the results for

Table 2. Properties for the softening and hardening behaviour of materials a to e. The stress-strain responses in uniaxial tension are shown in Figure 2.

	a	b	c	d	e
s_{ss}/s_0	1.0	0.79	0.79	0.79	0.79
C^R/s_0	0.0	0.0	0.059	0.059	0.059
N	∞	∞	6.3	12.6	∞

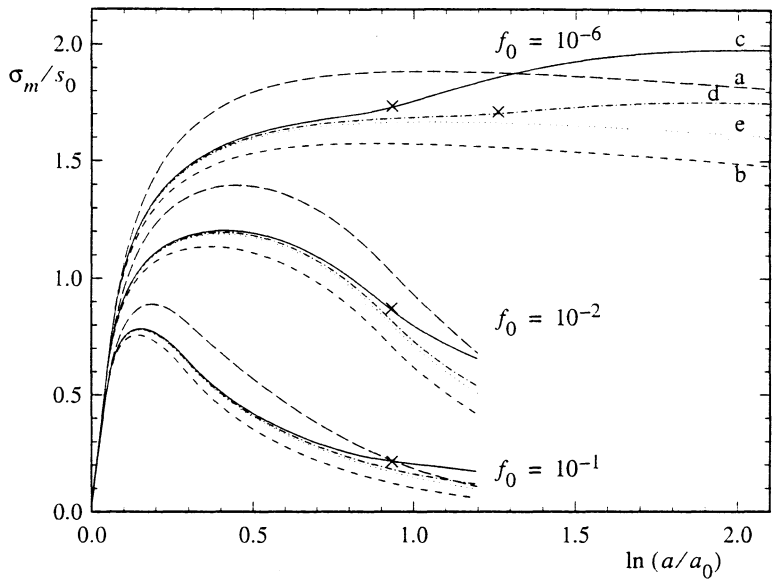

Figure 3. *Remote stress vs. void expansion, ln* (a/a_0)*, for various initial void volume fractions and parameters sets a and e. The crosses indicate the instant when network locking occurs at the inner radius* a.

materials a and b shows that softening tends to reduce the macroscopic yield stress, although the effect is never more than around 10%. The materials with hardening, according to sets c to e, show a behaviour which is intermediate to the response of a and b. A noteworthy feature of the response of materials c and d is the deviation away from that of material e after some of void expansion. This is due to the fact that after sufficient expansion, the limit stretch of the network, λ_{max}, is reached at the inner radius for materials c and d, as indicated in Figure 3.

In this case, the response will depend strongly on the assumptions underlying the material model. In terms of the one-dimensional model in Figure 1 which is employed here, this means that the Langevin spring is locked, which also prevents any further plasticity in the dashpot. Then, continued deformation can only be sustained elastically. Consequently, very high stresses are developed at the inner shell, but still the effect on the macroscopic stress is moderate, because the thickness of the shell for which network locking occurs remains thin. An alternative speculation could be that if the limit stretch is reached, continued deformation is governed by a disentanglement process, causing an increase of the hardening parameter N. In the current formulation of the material model, this behaviour is not accounted for. Modification of the material model could be done based on the stress and temperature induced network dissociation model by Raha and Bowden [19,20], but this is far beyond the scope of this paper.

The differences in response for the various materials can be understood by examination of the radial distribution of the shear stress. For an initial void volume fraction of $f_0 = 10^{-2}$, the stress distributions for materials a to e at a void expansion of $\ln(a/a_0) = 0.5$ are depicted in Figure 4. Yield, followed by softening and hardening has occurred inside the inner part of the sphere, while the outer part of the sphere is still elastic. It is seen that orientation hardening (materials c, d, and e) causes an elevation of the shear stress at the inner shell, compared to the pure softening material b. However, this effect decays rapidly because the strain gradient is very high at the inner shell and the shear stress distribution for the hardening materials approaches that of material b for larger radii. Also, the differences in the hardening parameter N for materials c, d, and e cause subtle differences in the shear stress at the inner shell. As these effects take place in a relatively thin zone near the inner radius, their influence on the macroscopic response in Figure 3 remains small.

The results for the macroscopic yield stress of materials a, b, and e with initial volume fraction f_0 ranging from 10^{-6} to 0.4 are confronted in Figure 5 with predictions assuming rigid-plastic material behaviour. The latter kind of analysis was proposed by McClintock and Stowers, and used later by Argon and Hannoosh [4] in their crazing study. In that case, the maximum remote stress at fully plastic flow, Σ_m, is derived from the infinitesimal strain version of Equation (4) as

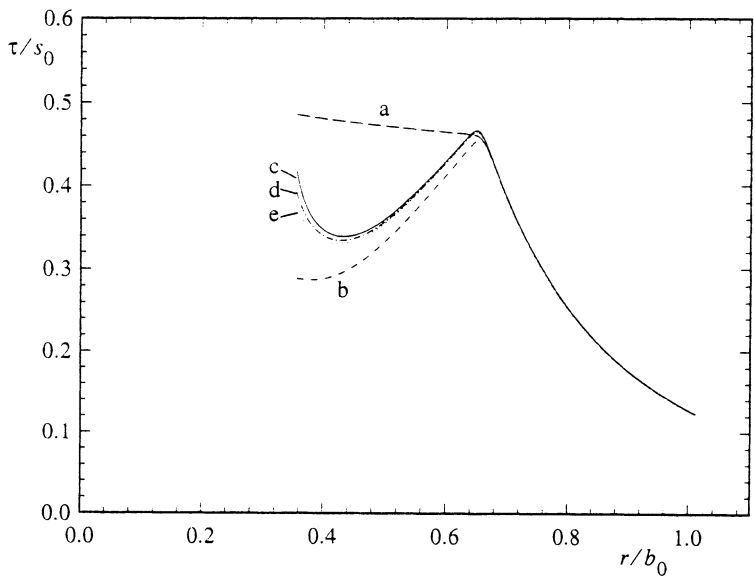

Figure 4. *Radial distribution of shear stress at the macroscopic yield point, i.e., at* $\ln(a/a_0) \approx 0.05$, *for an initial void volume fraction* $f_0 = 10^{-2}$, *and parameter sets a, b, e.*

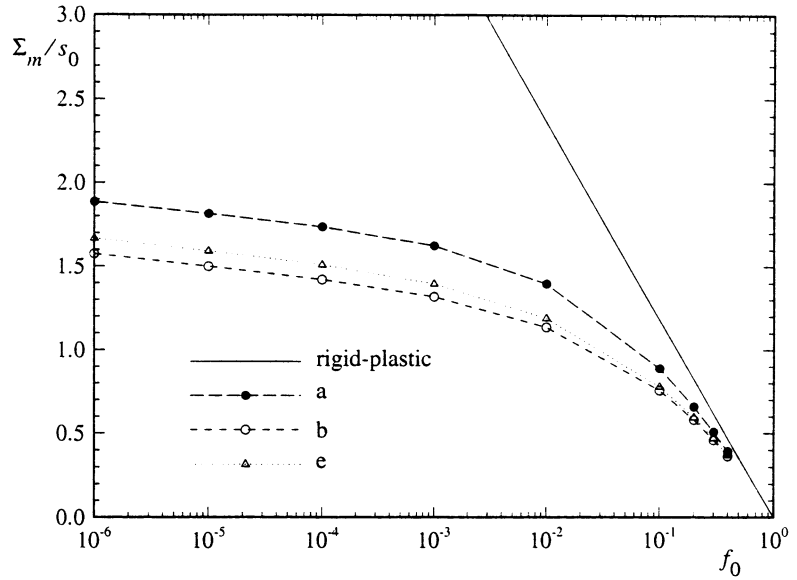

Figure 5. *Macroscopic yield stress vs. initial void volume fraction for parameter sets a, b, e compared with rigid-plastic behaviour.*

$$\frac{\Sigma_m}{s_0} = 2\sqrt{3}\int_{a_0}^{b_0}\left(\frac{\tau_F}{s_0}\right)\frac{dr}{r} = -\frac{2}{\sqrt{3}}\frac{\tau_F}{s_0}\ln f_0 \tag{12}$$

where τ_F is the (rate-independent) shear flow stress. This result coincides with Gurson's [12] model for purely hydrostatic stress states. The approximation of rigid-plastic material behaviour is usually appropriate for metals, but it can be seen that it does not yield accurate results in the case of glassy polymers. This is due to the relatively large strain at yield for most glassy polymers, which is typically between 5 to 10% (see, e.g., Figure 2), whereas in metals this is in the order of 0.1%. Hence, significant geometry changes occur prior to macroscopic yield in polymers, and part of the sphere is still elastic at macroscopic yield, as seen in Figure 4. This leads to significantly lower stresses than according to Equation (12), especially for smaller f_0, as discussed in Reference [9].

In particular, we notice that according to Equation (12), the remote stress is linear in $\ln f_0$, whereas the yield stress Σ_m based on the actual stress distribution according to Equation (4) levels off for low values of f_0. According to the actual stress distribution, it appears from Figure 5 that, in the limit of $f_0 \to 0$, the macroscopic yield stress remains finite. Thus, a cavitation instability is found, i.e., an initially infinitesimal void grows without bound, when this so-called

"cavitation limit" for Σ_m is reached. As discussed in detail in Reference [21] within the context of cavitation instabilities in metals, this instability relies on the availability of sufficient elastic energy remotely from the void to drive its growth. The phenomenon is a potential candidate for void nucleation in metals in conditions where high hydrostatic stresses can develop locally [21], and is essentially the same one as in Gent's [22] model for void nucleation in Neo-Hookean elastic rubbers.

Even though the uniaxial tension responses of materials a, b, and e are quite different (see Figure 2), the macroscopic yield point is not very much affected (see Figure 3), nor is the cavitation limit (see Figure 5). An estimate of the cavitation stress can then be obtained from the approximate solution obtained in Reference [9] for a material without softening and hardening (i.e., $h = 0$ and $C^R = 0$). In the limit of $f_0 \to 0$ this gives

$$\frac{\Sigma_m}{s_0} = \frac{2}{\sqrt{3}} \frac{\tau_b}{s_0} \ln\left(\frac{E}{\tau_b}\right) \tag{13}$$

with τ_b the equivalent shear stress necessary to sustain the equivalent shear rate $\dot{\gamma}_b = \sqrt{6}\dot{b}/b$ [see Equation (2)], at the outer boundary by plastic flow alone, i.e.,

$$\frac{\tau_b}{s_0} = \left[1 + \frac{T}{As_0} \ln\left(\frac{\dot{\gamma}_b}{\dot{\gamma}_0}\right)\right]^{6/5}$$

For the material parameters used here and for a remote strain rate of $\dot{b}/b = 0.01s^{-1}$, Equation (13) yields a cavitation stress of $\Sigma_m = 1.56s_0$.

In the foregoing, we have neglected the effect of surface tension inside the void. However, this may give a significant contribution for sufficiently small voids. This problem has been considered in the past by, for instance, References [6,23] for glassy polymers as well as for rubbery materials. For spherically symmetric voids, the surface tension γ can be simply incorporated by changing the boundary condition of Equation (3) into

$$\sigma_r(a) = \frac{2\gamma}{a} \qquad \sigma_r(b) = \sigma_m \tag{14}$$

This will introduce an additional threshold value for the macroscopic stress that depends on the size of the void or the sphere. A conceptual difficulty arises for infinitesimal voids, however, since Equation (14) leads to a singularity. In addition, it may be questioned if Equation (14) is indeed valid in the nucleation phase when the void size is close to molecular dimensions.

4. CONCLUSIONS

The effect of various features of yield in amorphous glassy polymers on the overall behaviour of a voided material has been investigated in terms of a simple hollow sphere model, similar to that used in References [12,9]. The macroscopic hydrostatic stress required for void growth is lower for softening materials, but the effect is quite limited. Also the strain hardening due to molecular orientation has a moderate effect on the macroscopic response. However, once the limit stretch of the molecular network is reached at the void radius, uncertainties remain in the model as to the subsequent behaviour of the material.

For the material parameter set used, typical for amorphous polymers like polycarbonate, the macroscopic yield stress of the porous material is significantly lower than in the case of a rigid-plastic matrix material, which forms the basis of the Gurson model. This is due to the fact that part of the sphere around the void is still elastic at the macroscopic yield point, especially for low void volume fractions. This effect is a consequence of the relatively large strain at yield in amorphous polymers. An approximate analytical solution of the yield stress was used in Reference [9] to modify Gurson's [12] yield potential for this effect.

The present model predicts a cavitation instability in yielding amorphous polymers. Depending subtly on softening and hardening characteristics, the cavitation limit is in the range of about 1.7 and 1.9 times the shear yield strength s_0. This is significantly lower than the values found for cavitation instabilities in metals [21], for the same reason mentioned above that the yield strain in polymer is an order of magnitude larger than for metals.

ACKNOWLEDGEMENTS

The work of A. C. Steenbrink is part of a research project funded by the Netherlands Technology Foundation (STW).

REFERENCES

1. Bucknall, C. B. 1977. *Toughened Plastics* (Applied Science Publ., London).
2. Donald, A. M. and E. J. Kramer. 1982. *J. Mat. Sci.*, 17:1765–1772.
3. Kambour, R. P. 1973. *J. Polymer Sci.: Macromolecular Reviews*, 7:1–154.
4. Argon, A. S. and J. G. Hannoosh. 1977. *Phil. Mag.*, 36:1195–1216.
5. Argon, A. S. and M. M. Salama. 1977. *Phil. Mag.*, 36:1217–1234.
6. Kramer, E. J. 1983. *Adv. Pol. Sci.*, 52/53:1–55.
7. Kramer, E. J. and L. L. Berger. 1990. *Adv. Pol. Sci.*, 91/92:1–67.
8. van der Giessen, E. and P. D. Wu. 1995. In *Mechanics of Plastics and Plastic Composites*, M. C. Boyce, ed., MD-Vol. 68/AMD-Vol. 215 (ASME, New York) pp. 203–221.
9. Steenbrink, A. C., E. van der Giessen and P. D. Wu. 1997. *J. Mech. Phys. Solids*, 45:405–437.
10. Tvergaard, V. 1990. *Adv. Appl. Mech.*, 27:83–151.
11. Lazzeri, A. and C. B. Bucknall. 1995. *Polymer*, 36:2895–2902.
12. Gurson, A. L. 1977. *J. Engng. Mater. Technol.*, 99:2–15.

13. Haward, R. N. and G. Thackray. 1968. *Proc. Roy. Soc. London,* A302:453–472.
14. Argon, A. S. 1973. *Phil. Mag.,* 28:839–865.
15. Boyce, M. C., D. M. Parks and A. S. Argon. 1988. *Mech. Mater.,* 7:15–33.
16. Arruda, E. M. and M. C. Boyce. 1993. *J. Mech. Phys. Solids,* 41:389–412.
17. Wu, P. D. and E. van der Giessen. 1993. *J. Mech. Phys. Solids,* 41:427–456.
18. Tomita, Y. and S. Tanaka. 1995. *Int. J. Solids Structures,* 32:3423–3434.
19. Raha, S. and P. B. Bowden. 1972. *Polymer,* 13:174–183.
20. Arruda, E. M., M. C. Boyce and R. Jayachandran. 1995. *Mech. Mater.,* 19:193–212.
21. Huang, Y., V. Tvergaard and J. W. Hutchinson. 1991. *J. Mech. Phys. Solids,* 39:223–241.
22. Gent, A. N. and P. B. Lindley. 1958. *Proc. Roy. Soc. London,* A249:195–204.
23. Gent, A. N. and D. A. Tompkins. 1969. *J. Pol. Sci. Part A-2,* 7:1483–1488.